Resonant cavity-enhanced quantum dot field-effect transistor as a single-photon detector*

Dong Yu(董 宇)[a)†], Wang Guang-Long(王广龙)[a)], Wang Hong-Pei(王红培)[a)], Ni Hai-Qiao(倪海桥)[b)], Chen Jian-Hui(陈建辉)[a)], Gao Feng-Qi(高凤岐)[a)], Qiao Zhong-Tao(乔中涛)[a)], Yang Xiao-Hong(杨晓红)[b)], and Niu Zhi-Chuan(牛智川)[b)]

[a)] *Laboratory of Nanotechnology and Microsystems, Mechanical Engineering College, Shijiazhuang* 050000, *China*
[b)] *Institute of Semiconductors, Chinese Academy of Sciences, Beijing* 100083, *China*

(Received 1 November 2013; revised manuscript received 10 February 2014; published online 10 August 2014)

A resonant cavity-enhanced (RCE) quantum dot (QD) field-effect transistor (RCEQDFET) is designed for single-photon detection in this paper. Adding distributed Bragg reflection (DBR) mirrors to the single-photon detector (SPD), we improve the light absorption efficiency of the SPD. The effects of the reflectivity of the mirrors, the thickness and light absorption coefficient of the absorbing layer on the detector's light absorption efficiency are investigated, and the resonant cavity is determined by using the air/semiconductor interface as the mirror on the top. Through analyzing the relationship between the refractive index of $Al_xGa_{1-x}As$ and Al component, we choose $AlAs/Al_{0.15}Ga_{0.85}As$ as the material of the mirror on the bottom. The pairs of $AlAs/Al_{0.15}Ga_{0.85}As$ film are further determined to be 21 by calculating the reflectivity of the mirror. The detector is fabricated from semiconductor heterostructures grown by molecular beam epitaxy. The reflection spectrum, photoluminescence (PL) spectrum, photocurrent response, and channel current of the detector are tested and the results show that the RCEQDFET-SPD designed in this paper has better performances in photonic response and wavelength selection.

Keywords: single-photon detector, quantum dot field-effect transistor, resonant cavity enhanced

PACS: 42.60.Da, 85.30.Tv, 85.60.Gz **DOI:** 10.1088/1674-1056/23/10/104209

1. Introduction

With the improvement of quantum communication, it is necessary to develop more sophisticated single-photon detector.[1–5] This is also crucial to scientific research in the areas of low light measurements in chemistry and astronomy, medical imaging, etc.[6,7] Several types of SPDs have been developed to date.

The first type of SPD includes photomultiplier tube (PMT) and avalanche photodiode (APD) which are based on external and internal photoelectric effects respectively. PMT mainly works for the visible light and ultraviolet and possesses low quantum efficiency at the infrared wavelength.[8] Many attempts have been made to improve the performance of APD especially in reducing the afterpulsing noise and increasing the gating rates.[9–11] Using the self-differencing technique, the quantum efficiency of APD can be enhanced considerably at high gating rates while the afterpulsing noise does not increase a lot.[12,13] However, as PMT and APD rely on the photo-multiplication principle, they both have the disadvantages of high dark count rate and low detection efficiency, and the detection wavelength of most instruments are restricted in a region of visible spectrum.[14–16]

Superconducting SPD (SSPD) including superconducting nanowire SPD (SNSPD) and transition edge sensor (TES) represents another type of SPD which is based on superconducting material sensitivity to the variation in temperature. The SSPD is suitable for operation at telecommunication wavelength with low dark count rate, high detection efficiency and speed. Recently, multichannel SSPD systems have been recognized as promising instruments which have been used in several areas such as optical communications, quantum optics, and quantum key distribution.[17–19] What is more, dividing the active area of the detector into multi-arrays is an attractive way to avoid the trade-off between the maximum counting rate and detection efficiency of the detector. The realization of large format SSPD arrays will have a great influence on various application fields.[20] However, the quantum communication requires the preservation of spin information of photogenerated carriers while the ones in SSPD are not obtainable. For this reason, SSPD is not suitable for single photon detection in quantum communication.[21,22]

By contrast, a new type of SPD based on quantum dot field-effect transistor can safely bound the photogenerated carriers, realizing spin coherent SPD.[23] QDFET-SPD uses a layer of quantum dots (QDs) as charge traps to confine the photogenerated carriers which are monitored by a transverse current flowing in a two-dimensional electron gas (2DEG).[24] In 2000, Shields *et al.*[25] reported the detection of single pho-

*Project supported by the National Natural Science Foundation of China (Grant No. 61274125) and the Natural Science Foundation of Beijing, China (Grant No. 11DB1262).

†Corresponding author. E-mail: jushangzhilei@foxmail.com

© 2014 Chinese Physical Society and IOP Publishing Ltd

tons based on GaAs/AlGaAs modulation-doped FET containing a layer of InAs QDs. The capture of single photoexcited carriers by QDs leads to measurable fluctuations of the source–drain current in their SPD. As the location of the absorbing region and QDs can be controlled independently, various active area sizes and dimensions can be realized in the fabrication of the QDFET-SPD with information uniformity and low dark count rate.[26] According to Ref. [27], a dark count rate of 0.003 Hz can be obtained with an internal quantum efficiency of 53±11%. For comparison, the dark count rate of APD is up to 16 Hz even after optimization.[28] Meanwhile, due to the confinement effect of QDs to the photogenerated carriers, the afterpulsing noise in the QDFET-SPD should be very low compared with APD.

While QDFET-SPD has high internal gain, its overall efficiency is merely 2∼3 percent.[29] It is mainly caused by the poor light absorption efficiency of QDFET-SPD while most of the light directly passes through the separator and enter into the substrate without being absorbed. To resolve this problem, a QDFET-SPD with a resonant cavity is proposed in our previous work[30] which significantly enhanced the light absorption of the detector at 800 nm. However, in our later tests of the photocurrent and photonic response, we find that the central working wavelength of the detector shifts a dozen of nanometers from 800 nm, the causation of which is possibly that the GaAs buffer affects the reflection effect of GaAs/AlAs films and the structural parameters of the detector are selected improperly. We therefore redesign an RCEQDFET-SPD by starting from the analysis of the influencing factors of the detector's light absorption efficiency. By enhancing the resonance of the light in the detector, the detector achieves enhancive light absorption efficiency as well as central working wavelength located around 800 nm.

2. Structure of the RCEQDFET-SPD

The structure of the RCEQDFET-SPD is shown in Fig. 1. The basic structure of the detector is a QDFET. A layer of QDs is injected between the gate and 2DEG. To obtain a higher carrier concentration and an electron mobility, an Si layer is doped via δ doping technology under the AlGaAs separator.

An absorbing layer and two distributed Bragg reflection (DBR) mirrors which together compose a resonant cavity are added to enhance the light absorption efficiency of the QDFET-SPD. The incident light is reflected back and forth, and made to interfere with each other in the cavity. By designing an appropriate cavity length, the optical intensity can be amplified remarkably at the wavelength of interest.[31–35] Meanwhile, as the mirror is placed between the separator and buffer, the formation of a second 2DEG is prevented. What is more, due to the resonance effect of two DBR mirrors, the RCEQDFET-SPD has the capability of selecting a wavelength which greatly reduces the noise jamming and the dark count rate. When the gate is at a bias voltage, the photogenerated holes will be trapped by the QDs. Then the photoconductance will increase greatly through the combined action of the resonant cavity and the modulation of the QDs, thereby realizing single-photon detection.

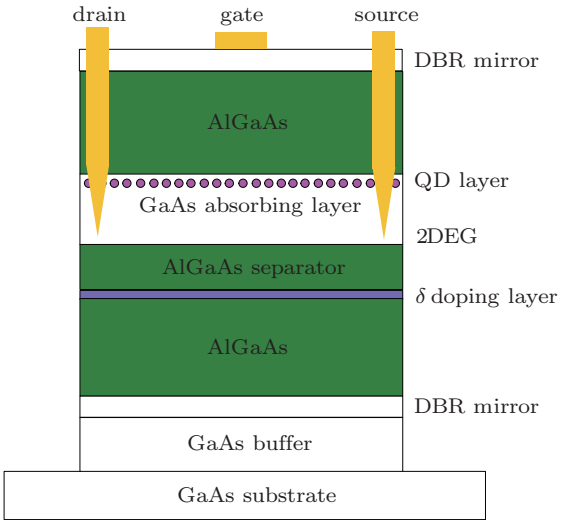


Fig. 1. (color online) Structure of the RCEQDFE-SPD.

3. Influencing factors of the light absorption efficiency of detector

The light absorption efficiency of the detector refers to the ratio of the power of the light absorbed by the absorbing layer (P_a) to the power of the incident light (P_i). The relationship[36] between P_a and P_i in the RECQDFET-SPD is as follows:

$$P_a = \frac{1+R_b e^{-\alpha d}}{1-2\sqrt{R_t R_b}\, e^{-\alpha d}\cos(2\beta L+\psi_t+\psi_b)+R_t R_b e^{-2\alpha d}} \times (1-R_t)\left(1-e^{-\alpha d}\right) P_i, \quad (1)$$

where R_t and R_b are the reflectivities of the mirrors on the top and bottom respectively, α and d are the light absorption coefficient, and thickness of the absorbing layer respectively, β is the propagation constant, L denotes the distance between two DBR mirrors, ψ_t and ψ_b denote the phase shifts induced by the optical transmission in the mirrors on the top and bottom respectively. Therefore, the light absorption efficiency of the detector can be denoted as

$$\eta = \frac{P_a}{P_i} = \frac{1+R_b e^{-\alpha d}}{1-2\sqrt{R_t R_b}\, e^{-\alpha d}\cos(2\beta L+\psi_t+\psi_b)+R_t R_b e^{-2\alpha d}} \times (1-R_t)\left(1-e^{-\alpha d}\right). \quad (2)$$

According to the theory of resonant cavity, the light absorption efficiency of the detector will reach a maximum value when $2\beta L+\psi_t+\psi_b = 2m\pi$. In this condition, the maximum light absorption efficiency of the detector can be expressed as

$$\eta_{max} = \frac{\left(1+R_b e^{-\alpha d}\right)}{\left(1-\sqrt{R_t R_b}\, e^{-\alpha d}\right)^2}(1-R_t)\left(1-e^{-\alpha d}\right). \quad (3)$$

From Eq. (3), we can figure out that the maximum light absorption efficiency of the detector is related to the reflectivities of the mirrors on the top and bottom, the light absorption coefficient, and thickness of the absorbing layer. For the convenience of analysis, αd in Eq. (3) is defined as normalized absorption coefficient which indicates the characteristic of the absorbing layer. Figure 2 shows the maximum light absorption efficiency variation when $R_t = 0.9$. In such a circumstance, only when R_b is large (larger than 0.9) and αd is small (smaller than 0.2) can the light absorption efficiency reach a relatively high value, therefore the reflectivity of the mirror on the top should not be designed to be too high. Therefore, we choose a scheme without a mirror on the top, and use the air/semiconductor interface instead, of which the reflectivity is about 0.3. When $R_t = 0.3$, the maximum light absorption efficiency variation is illustrated in. Fig. 3.

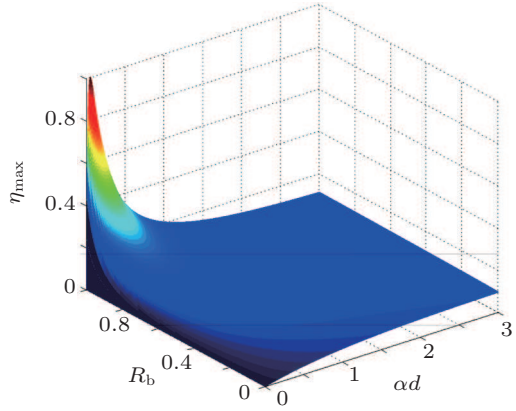


Fig. 2. (color online) Maximum light absorption efficiency variation when $R_t = 0.9$.

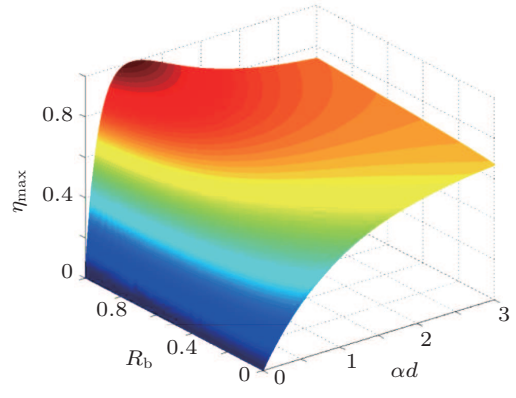


Fig. 3. (color online) Maximum light absorption efficiency variation when $R_t = 0.3$.

It is shown that the maximum light absorption efficiency changes when αd is between 0 and 1.5 and basically stabilizes at 0.7 when αd is larger than 1.5. What is more, the reflectivity of the mirror on the bottom should be larger than 0.5 to obtain a relatively high light absorption efficiency. To further analyze the effect of the reflectivity of the mirror on the bottom on the light absorption efficiency of the detector, the maximum light absorption efficiency is simulated when the values of αd are 0.05, 0.3, 0.6, 1, and 1.5. The results are shown in Fig. 4.

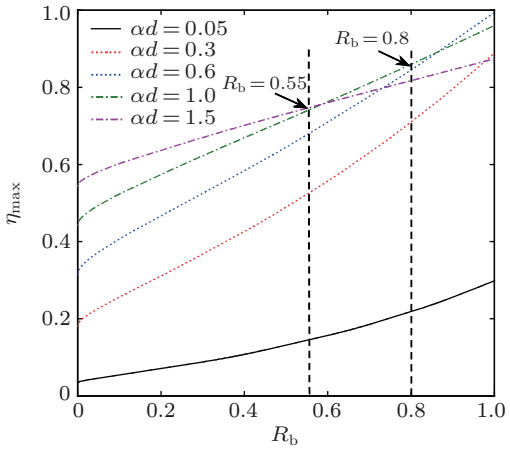


Fig. 4. (color online) Variations of maximum light absorption efficiency with reflectivity of the mirror on the bottom for several different values of αd (0.05, 0.3, 0.6, 1, and 1.5).

It is found that the maximum light absorption efficiency increases in turn with the increase of αd when R_b is smaller than 0.55. However, when R_b is larger than 0.8, the detector with αd being 0.6 has the best light absorption efficiency whose maximum value reaches 0.99.

4. Design of resonant cavity

From the above analysis, we can know that the reflectivity of the DBR mirror on the bottom has a great effect on the light absorption efficiency of the RCEQDFET-SPD. The reflectivity should be as high as possible in order to achieve better light absorption efficiency. In this paper, the DBR mirror is constructed by alternately growing $Al_xGa_{1-x}As$ film. We simulate the refractive indices[37] of $Al_xGa_{1-x}As$ when the Al components are 0.15, 0.9, and 1 as illustrated in Fig. 5. It is shown that the refractive index of $Al_xGa_{1-x}As$ has little difference when the Al components are 0.9 and 1, while it has relatively big difference when the Al components are 0.15 and 1. For the DBR mirror having higher reflectivity, the alternately grown $Al_xGa_{1-x}As$ films should have bigger difference in refractive index. Therefore, AlAs/$Al_{0.15}Ga_{0.85}As$ is chosen as the material of the mirror on the bottom. We can also figure out that each curve has two singularities due to the coincidence between the incident photon energy and the band gap of $Al_xGa_{1-x}As$ which causes intrinsic absorption. To avoid the material failure caused by this phenomenon, $Al_xGa_{1-x}As$ is unsuited for working at the wavelengths below the singularities.

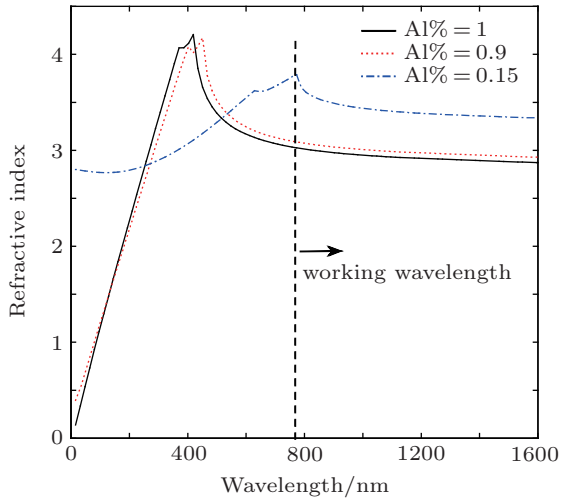


Fig. 5. (color online) Refractive index of $Al_xGa_{1-x}As$ when the Al component is 0.15, 0.9, and 1.

If there are k pairs of AlAs/$Al_{0.15}Ga_{0.85}As$, the reflectivity of the mirror on the bottom can be denoted as[38]

$$R_b = \left[\frac{1-(n_1/n_2)^{2k}}{1+(n_1/n_2)^{2k}}\right]^2, \tag{4}$$

where n_1 and n_2 denote the refractive indices of AlAs and $Al_{0.15}Ga_{0.85}As$ respectively. According to Eq. (4), the reflectivity of the mirror on the bottom is simulated, with the values of k being 10, 20, 21, and 25, and the results are illustrated in Fig. 6.

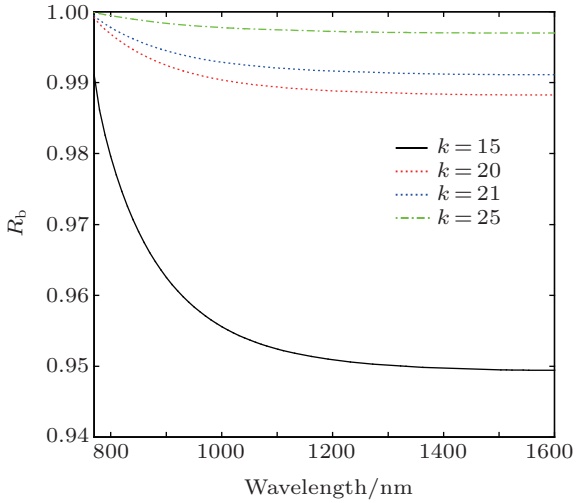


Fig. 6. (color online) Variations of reflectivity of the mirror on the bottom with wavelength, with the values of k being 10, 20, 21, and 25.

It is found that the reflectivity of the mirror on the bottom increases in turn with the increase of the pairs of AlAs/$Al_{0.15}Ga_{0.85}As$ at the working wavelength of the detector. At the beginning, they are all above 0.99 no matter what the value of k is, but the reflectivity of 15 pairs of AlAs/$Al_{0.15}Ga_{0.85}As$ decreases fast. At long-wave band, the reflectivity reaches $\sim$ 0.99 when $k = 20$ while it is totally above 0.99 when $k = 21$ and approaches 1 when $k = 25$. Owing to the fact that the barrier spike on the AlAs/$Al_{0.15}Ga_{0.85}As$ interface can lead to the increase of the series resistance of the mirror on the bottom, many AlAs/$Al_{0.15}Ga_{0.85}As$ pairs will reduce the performance of the detector in aspects of high-speed response, photoconductive gain, etc., and the pairs of AlAs/$Al_{0.15}Ga_{0.85}As$ are ultimately determined to be 21. Therefore the series resistance can be reduced as much as possible while the reflectivity is very high.

According to the analysis on Fig. 4, when R_b is 0.99, the normalized absorption coefficient of the absorbing layer should be designed to be 0.6 so as to reach the maximum light absorption efficiency. As the light absorption coefficient of GaAs which is chosen as the material of the absorbing layer is about 4×10^4 cm^{-1}, the thickness of the absorbing layer should be designed to be 150 nm.

5. Experimental results and discussion

Based on the above analysis, the RCEQDFET-SPD is fabricated from semiconductor heterostructures grown on GaAs substrates by molecular beam epitaxy, with 800 nm taken as its central working wavelength. The heterostructure layers consist of the following parts from the bottom to the top: 300-nm GaAs buffer, 21 pairs of AlAs/$Al_{0.15}Ga_{0.85}As$ films, 300-nm $Al_{0.26}Ga_{0.74}As$ barrier, δ doping layer, 30-nm $Al_{0.26}Ga_{0.74}As$ separator, 110-nm 2DEG, QD layer, 5-nm GaAs overcoat, 20-nm $Al_{0.26}Ga_{0.74}As$ blocking layer, 110-nm Si-doped (1.3×10^{15} cm^{-3}) $Al_{0.26}Ga_{0.74}As$ barrier, and 10-nm Si-doped (2.1×10^{18} cm^{-3}) GaAs contact layer.

Figure 7 shows the reflection spectrum and photoluminescence (PL) spectrum of the detector which are measured at room temperature. It is shown that the center of the high reflection band and the peak of PL intensity are located at 797 nm and 801 nm respectively, which only mismatch the central working wavelength of the detector slightly. The causation of this slight error may be that the thickness and flatness of AlAs/$Al_{0.15}Ga_{0.85}As$ film do not strictly accord with our theoretical design during the epitaxial growth. The PL intensity also has a relatively small peak at $\sim$700 nm, which is induced by the tunneling effect inside the detector. Except for the fluctuations at $\sim$ 700 nm and 801 nm, the PL spectrum almost remains stationary, no matter how the reflection varies, which proves the capability of wavelength selection of the RCEQDFET-SPD.

The photocurrent response of the detector at 0.3-V bias is illustrated in Fig. 8. As shown here, the curve peaks at 796 nm which basically matches the central working wavelength of the detector. Besides, there is a relatively small peak in wave band from 470 nm to 550 nm, the cause of which may be that the photon energy in this band is close to the GaAs barrier edge

and the escape rate of photogenerated carrier is quite high so that the photocurrent is enhanced.

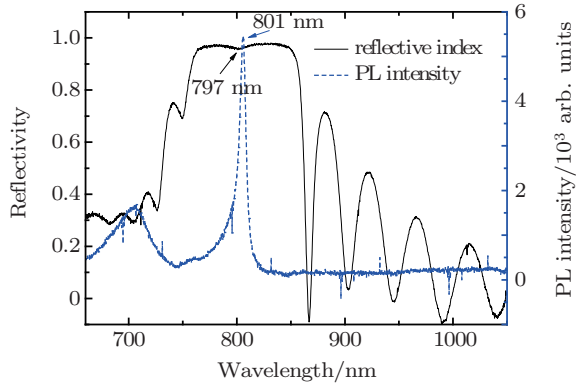


Fig. 7. (color online) Reflection spectrum and PL spectrum of the detector.

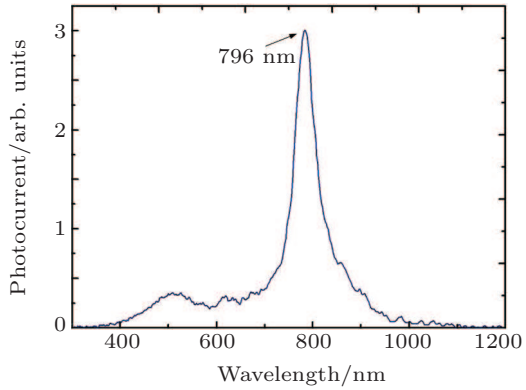


Fig. 8. (color online) Photocurrent response of the detector at 0.3-V bias.

For the purpose of testing the channel current of the detector, a single-photon source should be used for preciseness. In practice, many researchers[25,27,39,40] have approximately simulated the single-photon source by attenuating the LED or laser. In this paper, a wavelength tuning laser working at 800 nm with a repetition rate of 10 kHz is controlled to work for 20 ms, therefore a train of 200 photon bursts is emitted. The power of photon bursts is finally attenuated to 12×10^{-6} nW by 60-dB attenuation slices. Therefore, the average photon number of each burst is

$$c_{\rm p} = \frac{P_l}{h\omega r} = \frac{\lambda P_l}{chr} \approx 4.8, \tag{5}$$

where P_l and ω denote the power and frequency of the attenuated photon bursts respectively, h is the Planck constant, r is the repetition rate of the laser, c is the light velocity in vacuum, and λ is the wavelength of the light.

Figure 9 shows the channel currents of the detector. The measured value (solid line in Fig. 9(a)) has two spikes at the beginning and end of the curve which is caused by the gate reset operation. Once the photon stream arrives at ~10 ms, the channel current of detector rises continually until the photon stream ends. The measured value from 20 ms to 20.7 ms (marked with dotted ellipse in Fig. 9(a)) is magnified, which is shown in Fig. 9(b). It shows that the channel current actually rises in a stair-step manner while each step corresponds to one photon burst, namely ~ 4.8 photons averagely. However, different steps may correspond to different numbers of photons as the number of photons obeys the Poisson distribution. One photon burst with the number of photons less than the average value arouses a smaller step size than the average.

In Fig. 9(a), the dashed line represents the simulated channel current[40] of QDFET-SPD, which represents the best value a QDFET-SPD may achieve before adding resonant cavity. It can be obviously observed that the RCEQDFET-SPD can realize single photon detection effectively and both the slope and values of measured results are greater than the simulated ones, which indicates that the RCEQDFET-SPD designed in this paper has better photonic response than the one before optimization.

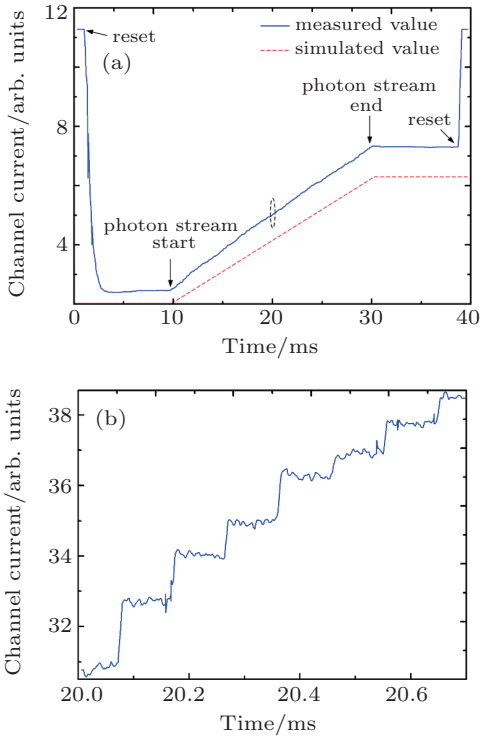


Fig. 9. (color online) (a) Channel current of the detector, and (b) magnified curve from 20 ms to 20.7 ms.

6. Conclusion

In this paper, we designed an RCEQDFET-SPD with the emphasis on enhancing the light absorption efficiency of detector. We proposed a scheme in which a 150-nm GaAs absorbing layer and a DBR mirror composed of 21 pairs of AlAs/$Al_{0.15}Ga_{0.85}As$ film are placed on the bottom of the detector to enhance the light absorption. Theoretically, the RCEQDFET-SPD has better light absorption efficiency and

wavelength selection at its working wavelength than the one before optimization. Practically, the center of the high reflection band, the peak of PL intensity, and photocurrent response of the experimental sample whose central working wavelength is designed to be 800 nm are located at 797 nm, 801 nm, and 796 nm respectively. Meanwhile, the measured channel current of the experimental sample indicates that the RCEQDFET-SPD realizes single photon detection effectively and performs better in photonic response and wavelength selection than the one before adding resonant cavity. The research results provide a new idea for designing a QDFET with high detection efficiency.

References

[1] Liu J, Wang Q, Kuang L M and Zeng H S 2010 *Chin. Phys. B* **19** 030313

[2] Wang T Y, Wen Q Y and Zhu F C 2009 *Chin. Phys. B* **18** 3189

[3] Baudot J, Dulinski W, Winter M, Barbier R, Chabanat E, Depasse P and Estre N 2009 *Nucl. Instrum. Methods Phys. Res. Sect. A: Accelerators, Spectrometers, Detectors and Associated Equipment* **604** 111

[4] Pan Z L, Chen L and Chen G J 2013 *Nucl. Instrum. Methods Phys. Res. Sect. B: Beam Interactions with Materials and Atoms* **307** 210

[5] Bouzid A, Park J B, Kim S M, Kwak S and Moon S 2011 *Curr. Appl. Phys.* **11** 903

[6] Vilella E, Alonso O, Montiel A, Vilà A and Diéguez A 2013 *Sensors and Actuators A: Physical* **201** 342

[7] Gys T 2008 *Nucl. Instrum. Methods Phys. Res. Sect. A: Accelerators, Spectrometers, Detectors and Associated Equipment* **595** 136

[8] Acerbi F, Tosi A and Zappa F 2013 *Sensors and Actuators A: Physical* **201** 207

[9] Lunghia T, Barreiroa C, Guinnarda O, Houlmanna R, Jiangb X, Itzlerb M A and Zbindena H 2012 *J. Mod. Opt.* **59** 1481

[10] McCarthy A, Krichel N J, Gemmell N R, Ren X, Tanner M G, Dorenbos S N, Zwiller V, Hadfield R H and Buller G S 2013 *Opt. Express* **21** 8904

[11] McCarthy A, Ren X, Frera A D, Gemmell N R, Krichel N J, Scarcella C, Ruggeri A, Tosi A and Buller G S 2013 *Opt. Express* **21** 22098

[12] Nambu Y, Takahashi S, Yoshino K, Tanaka A, Fujiwara M, Sasaki M, Tajima A, Yorozu S and Tomita A 2011 *Opt. Express* **19** 20531

[13] Warburton R E, Intermite G, Myronov M, Allred P, Leadley D R, Gallacher K, Paul D J, Pilgrim N J, Lever L J M, Ikonic Z, Kelsall R W, Huante-Ceron E, Knights A P and Buller G S 2013 *Electron. Dev.* **60** 3807

[14] Liu Y, Wu Q L, Han Z F, Dai Y M and Guo G C 2010 *Chin. Phys. B* **19** 080308

[15] Wang J, Wei Z J, Wang G, Guo L, Wang J D, Zhang Z M, Guo J P, Guo B H and Liu S H 2013 *Acta Phys. Sin.* **62** 014203 (in Chinese)

[16] Alexeev M, Birsa R, Bradamante F, *et al*. 2010 *Nucl. Instrum. Methods Phys. Res. Sect. A: Accelerators, Spectrometers, Detectors and Associated Equipment* **623** 129

[17] Rosenberg D, Kerman A J, Molnar R J and Dauler E A 2013 *Opt. Express* **21** 1440

[18] Natarajan C M, Zhang L, Coldenstrodt-Ronge H, Donati G, Dorenbos S N, Zwiller V, Walmsley I A and Hadfield R 2013 *Opt. Express* **21** 893

[19] Shibata H, Shimizu K, Takesue H and Tokura Y 2013 *Appl. Phys. Express* **6** 072801

[20] Hu X, Zhong T, White J E, Dauler E A, Najafi F, Herder C H, Wong F N C and Berggren K 2009 *Opt. Lett.* **34** 3607

[21] Zhang L B, Kang L, Chen J, Zhao Q Y, Jia T, Xu W W, Cao C H, Jin B B and Wu P H 2011 *Acta Phys. Sin.* **60** 038501 (in Chinese)

[22] Miki S, Yamashita T, Terai H, Makise K, Fujiwara M, Sasaki M and Wang Z 2012 *Phys. Procedia* **36** 77

[23] Li Y Q, Wang X D, Xu X N, Liu W, Yang F H and Zeng Y P 2011 *Physica E: Low-dimensional Systems and Nanostructures* **44** 686

[24] Tabe M, Udhiarto A, Moraru D and Mizuno T 2011 *Phys. Status Solidi A* **208** 646

[25] Shields A J, O'Sullivan M P, Farrer I, Ritchie D A and Hogg R A 2000 *Appl. Phys. Lett.* **76** 3673

[26] Rowe M A, Salley G M, Gansen E J, Etzel S M, Nam S W and Mirin R P 2010 *J. Appl. Phys.* **107** 063110

[27] Rowe M A, Gansen E J, Greene M, Hadfield R H and Harvey T E 2006 *Appl. Phys. Lett.* **89** 253505

[28] Dixon A R, Yuan Z L, Dynes J F, Sharpe A W and Shields A J 2008 *Opt. Express* **16** 18790

[29] Gansen E J, Rowe M A, Greene M B, Rosenberg G D, Harvey T E, Su M Y, Hardfield R H, Nam S W and Mirin R P 2007 *Nat. Photon.* **1** 585

[30] Wang H P, Wang G L, Ni H Q, Xu Y Q, Niu Z C and Gao F Q 2013 *Acta Phys. Sin.* **62** 194205 (in Chinese)

[31] Guo J C, Zuo Y H, Zhang Y, Ding W C, Cheng B W, Yu J Z and Wang Q M 2009 *Chin. Phys. B* **18** 2223

[32] Chen C, Zhao L J, Qiu J F, Liu Y, Wang W and Lou C Y 2012 *Chin. Phys. B* **21** 094208

[33] Lee C T and Ho H W 2013 *Solid-State Electron.* **89** 153

[34] Dutta H S and Das N R 2012 *Procedia Technology* **4** 9

[35] Felder F, Fill M, Rahim M, Zogg H, Quack N, Blunier S and Dual J 2010 *Phys. Procedia* **3** 1127

[36] Schulz W M, Eichfelder M, Reischle M, Kessler C, Robbach R, Jetter M and Michler P 2011 *J. Cryst. Growth* **315** 127

[37] Montes M, Guzmán A, Trampert A and Hierro A 2010 *Solid-State Electron.* **54** 492

[38] Zhou J P, Wang M and Han D F 2009 *Int. J. Light Electron Opt.* **120** 987

[39] Kosaka H, Rao D S, Robinson H D, Bandaru P, Makita K and Yablonovitch E 2003 *Phys. Rev. B* **67** 045104

[40] Gansen E J, Rowe M A, Greene M B, Rosenberg D, Harvey T E, Su M Y, Hadfield R H, Nam S W and Mirin R P 2007 *IEEE J. Selec. Topics Quantum Electron.* **13** 967